frontiers | Frontiers in Future Transportation

TYPE Original Research
PUBLISHED 09 September 2022
DOI 10.3389/ffutr.2022.890776

OPEN ACCESS

EDITED BY
Robert Thomson,
Chalmers University of Technology, Sweden

REVIEWED BY
Jie Wang,
Changsha University of Science and Technology, China
Di Pan,
Xiamen University, China
Yong Han,
Xiamen University of Technology, China
Bengt Pipkorn,
Autoliv, Sweden
Chengyue Jiang,
Chongqing University of Technology, China

*CORRESPONDENCE
Wenle Lv,
lvwenle@tust.edu.cn

SPECIALTY SECTION
This article was submitted to Transport Safety,
a section of the journal
Frontiers in Future Transportation

RECEIVED 06 March 2022
ACCEPTED 26 July 2022
PUBLISHED 09 September 2022

CITATION
Li H, Lv W, Hynčík L, Zhou B, Zhao H, Cui S, He L and Ruan S (2022), Injury study of the 6-year-old pediatric thorax and abdomen in frontal sled tests using different computational models.
Front. Future Transp. 3:890776.
doi: 10.3389/ffutr.2022.890776

Injury study of the 6-year-old pediatric thorax and abdomen in frontal sled tests using different computational models

Haiyan Li[1], Wenle Lv[1]*, Luděk Hynčík[2], Bingbing Zhou[3], Hongqian Zhao[1], Shihai Cui[1], Lijuan He[1] and Shijie Ruan[1]

[1]Tianjin University of Science and Technology, Tianjin, China, [2]University of West Bohemia, Pilsen, Czechia, [3]Tianjin Quadrant Space Science and Technology Company, Limited, Tianjin, China

The correct use of a child restraint system (CRS) is an effective internationally recognized measure to protect the safety of child occupants which can reduce the probability of child road traffic accident deaths by 54–80%. Finite element (FE) analysis is one important method with which to study the protection of child occupants. The aim of this study was to investigate thoracic and abdominal injuries and the protective effect of CRS on child occupants in 6-year-old (6YO) children in a frontal sled test using different computational models. In this study, a verified FE model of a 6YO child occupant was placed in the FE model of a CRS with a three-point safety belt. In the simulation setup phase, the frontal sled simulation of the 6YO FE model was reconstructed by applying the AAMA pulse. Based on the simulation data of the Q6 dummy FE model (Q6) and the 6YO child Virthuman model (V6) from previous studies, the frontal sled test simulation of a verified 6YO child FE model with detailed anatomical structures (TUST IBMs 6YO) was carried out to analyze pediatric thorax and abdomen injuries under the same experimental conditions. According to the simulation results, the variation tendencies of the simulation responses such as chest acceleration and compression are consistent with each other, which can provide effective information for the design of a CRS. In addition, the simulation results of the TUST IBMs 6YO can provide a variety of simulation data, such as the maximum first principal strain value and nephogram, of the internal organs of the chest and abdomen, providing a theoretical basis for the performance analysis and later development of a CRS.

Abbreviations: AAMA, American Automobile Manufacturers Association; AIS, abbreviated injury scale; CRS, child restraint system; CT, computed tomography; ECER129, Economic Commission for Europe Regulation; FE, finite element; TUST IBMs 6YO, 6YO child FE model with detailed anatomical structures developed by Tianjin University of Science and Technology; HIC, head injury criterion; MBS, multibody system; PIPER, position and personalize advanced human body models for injury prediction; Q6, Q6 child dummy FE model; THUMS 3YO, total human model for safety 3-year-old; V6, virtual 6YO child model developed by automatic scaling; VC, viscous criterion.

KEYWORDS

child seat, occupant kinematics, frontal impact, chest and abdominal injury, finite element

1 Introduction

Cars have become a necessity for most families, and the use of CRS is gradually attracting the attention of young parents nowadays. Use of child dummies in sled tests is becoming more and more widespread in the later verification process of CRS design in spite of the limitations of the low recycling rate of dummies and large testing costs for enterprises. In addition to child dummies, multibody system (MBS) models are also widely used in CRS verification, while a child FE model with a detailed anatomy can better reflect the performance of the CRS, greatly reduce the costs of testing using numerical simulation, and be recycled during product development and upgrading.

Maňas et al. (2012) introduced the kinematic response and verification process of an MBS human model in a collision and explained its advantages and importance. Two kinds of MBS models, EUROSID 2 (fine model) and USSID (rough model), were introduced by Franz and Graf, 2000, where the materials were described in detail. A new type of CRS was introduced, and the performance of the seat model under the conditions of a frontal collision was studied by Cao et al. (2010), where it was shown that the seat can effectively protect children aged 3 and 6 years. In the study by Huang et al. (2016), it was found that the head displacement of the child MBS model was not sensitive to the waveform, but the pulse shape had a greater impact on the head and chest accelerations.

CRS research in developed countries in Europe and America started earlier, and the technology was more mature than that in China. Sled tests of 3- and 6-year-old children with a three-point safety belt and CRS were conducted in Beauchamp et al., 2005. With regard to the improvement of new test methods for CRS, Trosseille et al. (2001) studied the knowledge about child behavior and tolerance in the CREST project and put forward a new test procedure to determine the effectiveness of instrumentation. Jager et al., 2005 introduced earlier the feasibility of Q dummy series models in frontal impacts. Eggers et al. (2015) evaluated the safety of child occupants in the rear seats of vehicles through Q6 and Q10 dummies and concluded that the Q6 thorax was greatly affected by geometric parameters such as the safety belt and that the Q6 dummy can more truly reflect the injury mechanism of the thorax. Beillas et al. (2014) concluded that an upper deflection sensor can better evaluate the chest injury of the Q6 dummy by comparing the injury of the Q6 dummy with that of the FE model. Kim et al. (2014) conducted a sled test with the Economic Commission for Europe Regulation 129 (ECE R129) standard seat and Q6 child dummy seat and concluded that the safety belt anchor point can affect child injuries. Zhang et al. (2021) studied the effect of the belt restraint path on child occupant injury by reconstructing a sled test with a Q6 dummy model, and the simulation results showed that an optimized seat belt restraint path can effectively enhance the safety of child occupants. Maheshwari et al. (2019) compared and analyzed the responses of a Q6 child occupant FE model restrained in three types of CRS conditions on the FMVSS 213 test bench.

In terms of research into child chest injury, Ouyang et al. (2006) studied children in different age groups in frontal impact experiments. Due to the limitations of cadaver experiments, the researchers studied injury by developing FE models for simulation analysis. A 3-year-old child chest and abdomen FE model for the injury study was built by scaling the adult FE model based on measurements and statistics in Mizuno et al. (2005). Another method of model construction was to construct the chest and abdomen FE models with the actual human anatomical structures based on human computed tomography (CT) images. A detailed 10-year-old child chest FE model was developed and verified by reconstructing of a static loading experiment by Jiang. (2013). Lv et al. (2015) constructed a complete FE model of a 6-year-old (6YO) child pedestrian (FEM6) with detailed anatomical structures and verified it by reconstructing experiments and studying chest injury in lateral impacts, laying the foundation for the follow-up research of CRS. All these studies showed that a high biofidelic child FE model, which was scarce for 6YO child occupants, was a more realistic and reliable method for assessing child safety protection and injury. Therefore, it is necessary to investigate the effect of CRS on child injury with an intact 6YO occupant FE model, which has a realistic and detailed anatomical structure.

The present paper aims to study 6YO pediatric occupant thorax and abdomen injuries in terms of acceleration, deflection, and force utilizing a verified TUST IBMs 6YO in frontal sled simulations, which compares the results with those from the Q6 and V6 models obtained from Hyncik et al.'s study (2014) and the protective effect of CRS on child occupants. The first principal strain is regarded as an evaluation index to predict the injury of internal organs.

2 Model construction and simulation setup

The child biomechanical dummy is represented by the validated Q6 model (as reference); therefore, the comparison to this model corresponds to the comparison to the child dummy. Based on the numerical simulations of the Q6 dummy FE model and the V6 MBS model (Hyncik et al., 2014), the frontal sled test simulation of the verified TUST IBMs 6YO was carried out under the same experimental conditions.

TABLE 1 Dimensions of the 6YO child in this paper and the international standard.

Parameter	6YO child FE model	6YO child in the 50th percentile
Height (mm)	1135	1113
Mass (kg)	23.9	18.9
Chest width (mm)	207.4	216
Chest thickness (mm)	130.7	147
Chest circumference (mm)	573.8	598

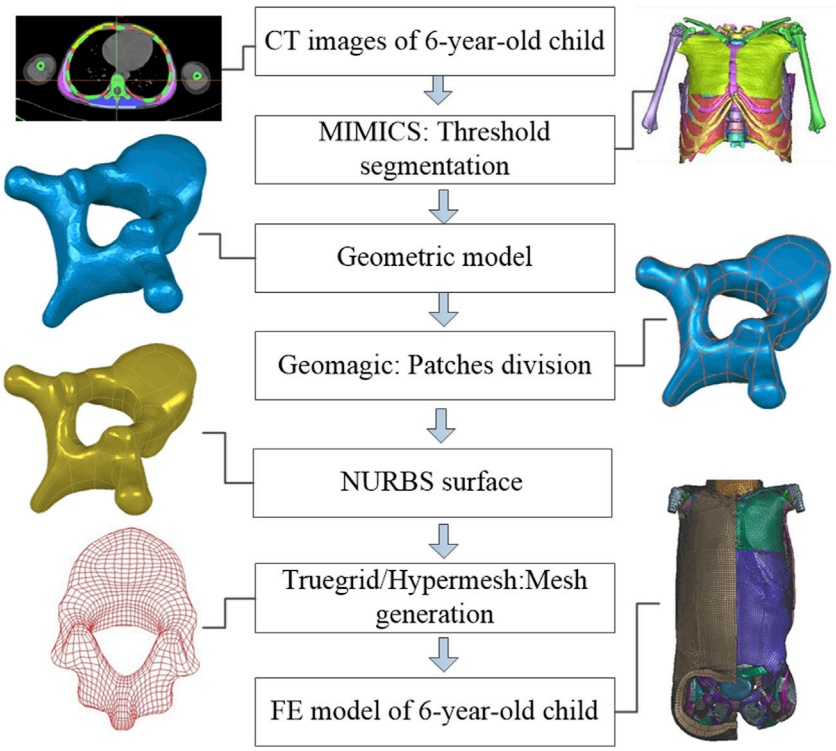

FIGURE 1
Construction process of pediatric FE model.

2.1 6-year-old child model

The TUST IBMs 6YO adopted in this paper conforms to the 50th percentile of the 6YO children's standard Human dimensions for Chinese minors, GB/T26158. The model is 1135 mm in height, 23.9 kg in weight, 207.4 mm in chest width, 130.7 mm in chest thickness, and 573.8 mm in chest circumference, as shown in Table 1.

The construction process for the child finite element model is as follows: first, the geometric model was extracted in Mimics 10.01 software by using the threshold segmentation method based on CT images of a 6YO child. The seated posture of the geometric model was obtained by rotating each part according to the seat angle. Then the geometric model was smoothed and divided into patches to obtain a patch model by using Geomagic 8.0. Finally, the FE model was constructed based on the geometric model by using Truegrid v2.1.0 and Hypermesh 12.0. In the FE model, cancellous bone, internal organs, muscle, fat, the spinal cord, cartilage, intervertebral discs, and other tissues were modeled by a hexahedral solid element, while cortical bone, ligament, skin, and the end plate were modeled by a shell element. The vertebral body was

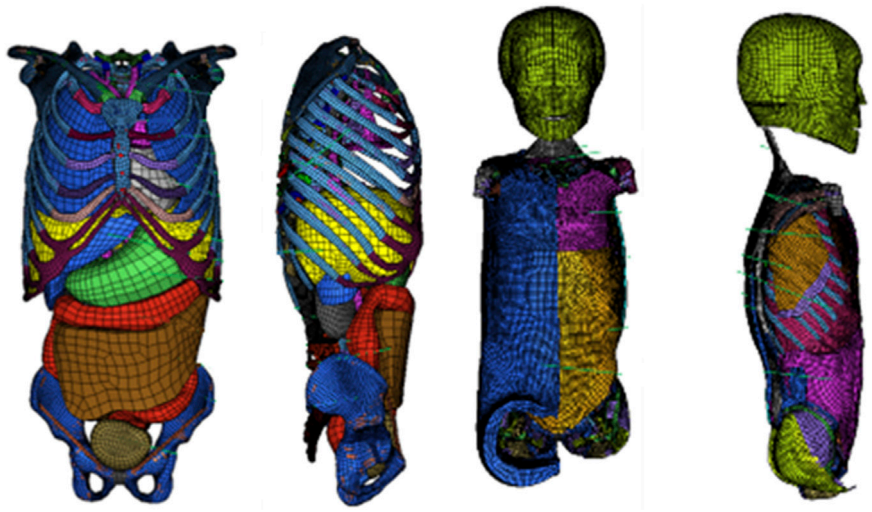

FIGURE 2
FE models of chest and abdomen of TUST IBMs 6YO including bones and internal organs (left) and muscle (right).

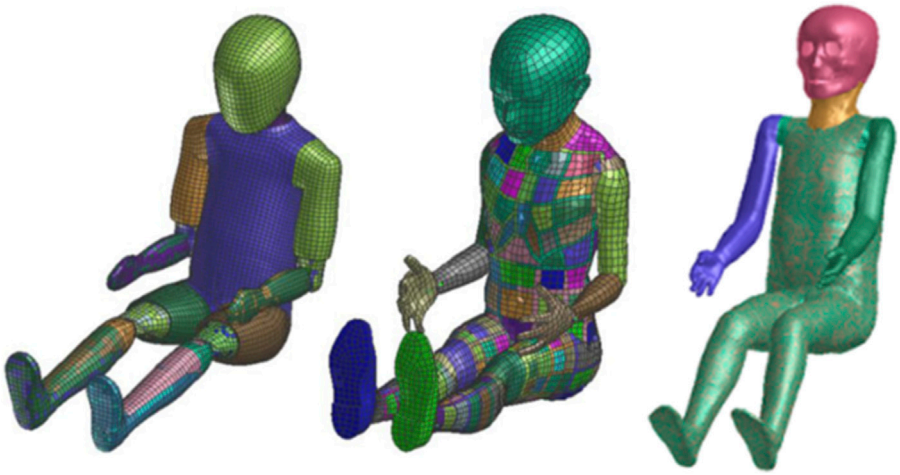

FIGURE 3
Q6 child dummy model (left). V6 child Virthuman model (middle) and TUST IBMs 6YO (right).

connected with the intervertebral disc by common nodes, which was the same for the connection between bone and muscle, skin, and fat. The contact between viscera and bone and different viscerae was defined as the surface–surface contact. The detailed construction process of the pediatric FE model is shown in Figure 1.

The material properties used in the 6YO child FE model were obtained from the literature (Untaroiu et al., 2005; Zhao and Norwani, 2007; Jiang et al., 2012; Lv et al., 2015; Lv WL. et al., 2016; Li et al., 2017a) and obtained by scaling adult material properties, which are summarized in Supplementary Appendix SA by Li et al. (2020). It should be noted that the scaling factor was obtained based on the existing child and adult tissue material parameters. The validity of the 6YO child FE model was verified by reconstructing several cadaver experiments (see Supplementary Appendix SB), and the simulation results were in good agreement with the experimental data, which indicated that this scaling method was feasible and reasonable to obtain child material under current conditions.

TABLE 2 Model data for the 6YO child.

Parameter	Q6	V6	TUST IBMs 6YO
Sitting height (mm)	601	653	671
Shoulder height (mm)	362	395	372
Shoulder width (mm)	305	262	217
Chest depth (mm)	141	180	172
Hip width (mm)	223	200	229
Buttocks to knee (mm)	366	350	315

The number of elements in the thorax and abdomen of TUST IBMs 6YO is 236,507. The model includes internal organs, skeletal tissues, muscles, ligaments, skin, and fat, as shown in Figure 2, which had been verified through the reconstruction of frontal impacts at different velocities (Ouyang et al., 2006; Ouyang et al., 2015) and lateral impact experiments at several angles (Shaw et al., 2006; Viano et al., 1989) in the literature (frontal impacts: Lv et al., 2015; Cui et al., 2016; lateral impacts: Lv et al., 2016b). Detailed information of the 6YO child FE model validation at the sub-model level is summarized in Supplementary Appendix SB by Li et al. (2020).

Figure 3 shows the Q6 child dummy model., 2013, the V6 child Virthuman model, and the TUST IBMs 6YO. The weight of the Q6 dummy is 22.98 kg, and the height is 1143 mm. The V6 child Virthuman model has a height of 1140 mm and a weight of 19 kg, which was obtained by scaling an adult model according to the relevant database of 6–7-year-old child heights (Hyncik et al., 2014).

The V6 child takes a step forward in human body modeling. V6 is a child human body model developed from an adult human body model (Vychytil et al., 2014) by a scaling algorithm based on actual anthropometric data (Hyncik et al., 2013). Both the geometry and stiffness are scaled to reconstruct a 6YO child's biomechanical properties. The model has been previously validated (Hyncik et al., 2013, 2014).

The TUST IBMs 6YO model was a finite element model of a 6YO child with detailed anatomical structures based on CT data. The V6 model was a special hybrid model that benefits from combining the MBS approach with deformable elements to enable injury assessment for a variety of impacts. The Q6 model was a full finite element model developed by Humanetics (2013), including inner and outer segments as a virtual copy of the physical Q6 child dummy, which was validated to correspond to the Q6 physical dummy response (Humanetics, 2013).

Body size is an important parameter for collision analysis, and the body sizes are shown in Table 2. The corresponding relationship can be effectively analyzed by body size. According to the size data of the three child models, each model has its own characteristics. The child FE model has a lower shoulder width, while other data correspond to each other.

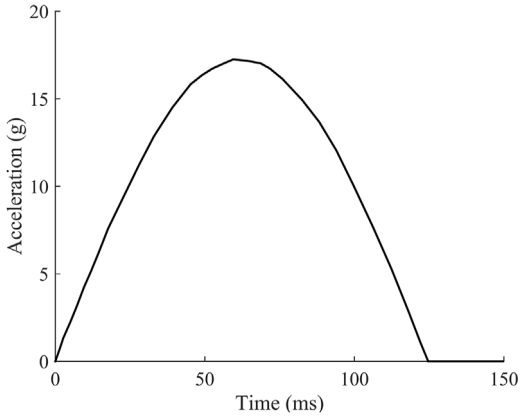

FIGURE 4
Frontal sled-AAMA sled pulse (the reproduce of the curve has been approved by the author Hyncik).

2.2 Safety seat FE model

In this paper, the FE model of CRS was built based on the geometric model of a child safety seat currently on the market using the pre-processing software HyperMesh 12.0. It consists of 1,231,296 elements, 32,570 shell elements, and 1,198,726 solid elements. The majority of the safety seat components were modeled by solid elements. The contact (*SYMMETRIC NODE-TO-SEGMENT WITH EDGE TREATMENT) in Pam-Crash software was used to model the boundary condition between the safety seat back portion and vehicle seat. The majority of the safety seat body was modeled as plastic material, while the padding was modeled as foam material. Furthermore, the three-point safety belt for a vehicle is built for the CRS, which is made of elastic isotropic material.

2.3 Simulation setup

The frontal sled simulation of the 6YO FE model was reconstructed by loading with the American Automobile Manufacturers Association (AAMA) pulse (Franz and Graf, 2000) (see Figure 4) in Virtual Performance Solutions 8.0. The simulation setup of the 6YO FE model was consistent with those of Q6 and V6 model simulations.

The sled consists of an ECE R16 seat. The sled and the seat models are taken from previous studies (Hyncik et al., 2014). The model is positioned in the seat, and a sliding contact interface (*SYMETRIC NODE-TO-SEGMENT WITH EDGE TREATMENT) is defined between the body and the seat. A three-point belt system is developed to model a C-pillar mounted belt restraint system. The simulation setups of the virtual 6YO child model and FE model are shown in Figure 5.

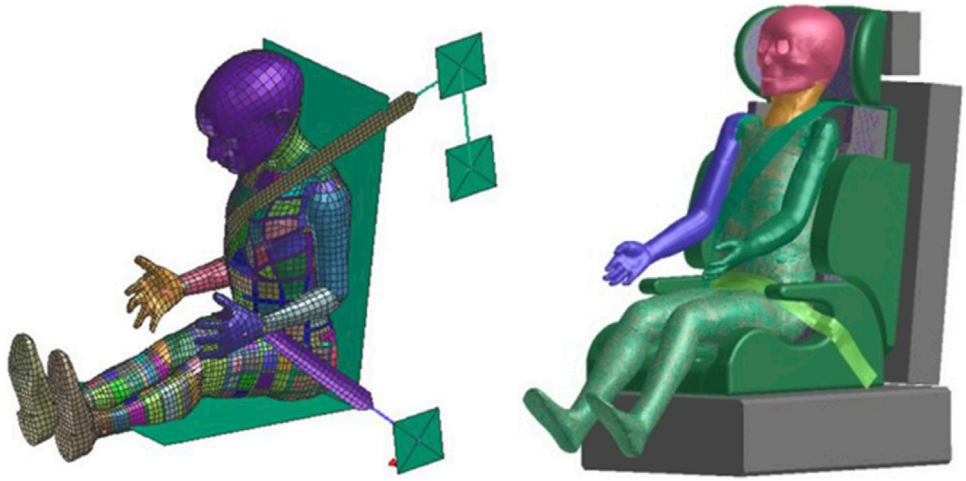

FIGURE 5
V6 (left) and TUST IBMs 6YO (right) in the frontal sled simulations (the reproduce of the Figure about V6 has been approved by the author Hyncik).

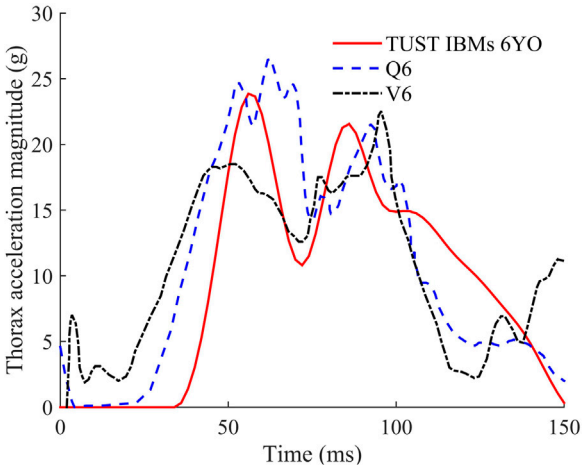

FIGURE 6
Thorax acceleration curves in frontal sled simulations.

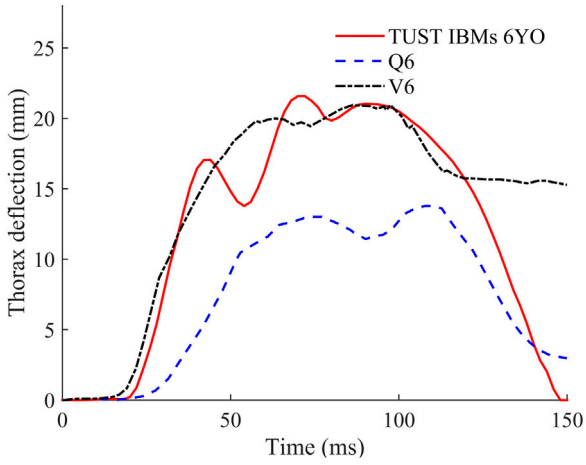

FIGURE 7
Thorax deflection curves in frontal sled simulations.

3 Results and discussion

The thorax acceleration, thorax deflection, shoulder belt force, and lap belt force curves obtained from the simulation results are compared with the corresponding curves of Q6 and V6 obtained from Hyncik et al.'s study (Hyncik et al., 2014), as shown in Figure 6, Figure 7, Figure 8, and Figure 9, and the reproduction of the curves was approved by the author Hyncik.

From Figures 6–9 and Table 3, it can be seen that there are two obvious peaks in the thorax acceleration curves of TUST IBMs 6YO, Q6, and V6, particularly 21.56 g/23.86 g, 21.52 g/27 g, and 23 g/18.51 g, respectively, while the maximum thorax accelerations are 23.86, 27, and 23 g, respectively. The variation tendency of the thorax acceleration curve of TUST IBMs 6YO agrees with those by Han et al. (2017) and Peng (2017), where simulations with a total human model for safety 3-year-old (THUMS 3YO) child FE model showed greater maximum thorax accelerations (Han et al., 2017). Possible reasons for the difference in maximum thorax acceleration could be associated with body weight and soft tissue energy absorption levels.

According to the variation tendencies of thorax deflection curves of TUST IBMs 6YO, Q6, and V6, there are two obvious peaks of 17.05 mm/21.58 mm, 14 mm/13, and 19.72 mm/21 mm in the corresponding curves, respectively. The maximum thorax

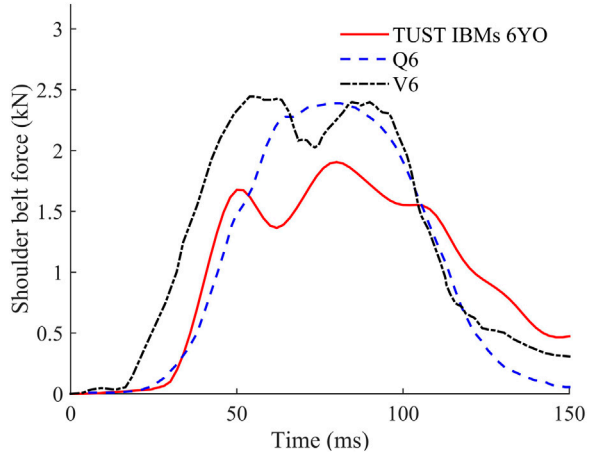

FIGURE 8
Shoulder belt force curves in frontal sled simulations.

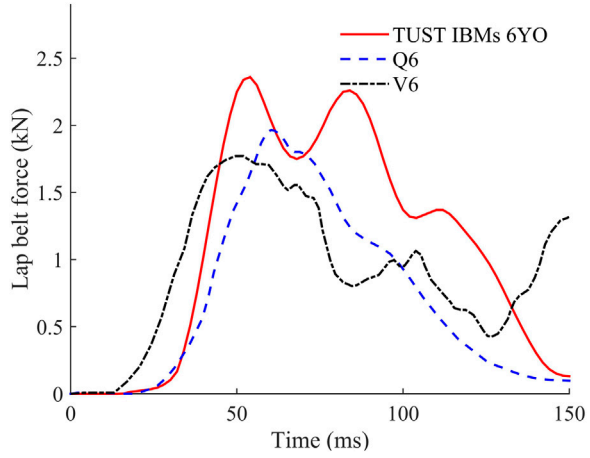

FIGURE 9
Lap belt force curves in frontal sled simulations.

TABLE 3 Maximum values for TUST IBMs 6YO, V6, and Q6.

Parameter	TUST IBMs 6YO	V6	Q6
Maximum thorax acceleration (g)	23.86	23	27
Maximum thorax deflection (mm)	21.58	21	14
Maximum shoulder belt force (kN)	1.91	2.53	2.48
Maximum lap belt force (kN)	2.36	1.77	1.96

deflections are 21.58, 14, and 21 mm in TUST IBMs 6YO, Q6, and V6, respectively. The maximum shoulder/lap belt forces of TUST IBMs 6YO, Q6, and V6 are 1.91 kN/2.36 kN, 2.48 kN/1.96, and 2.53 kN/1.77 kN, respectively. The maximum shoulder/lap belt load values of TUST IBMs 6YO (1.91 kN/2.36 kN) were much greater than those from low-speed, non-injurious frontal sled tests, which were conducted using male human volunteers with the sled acceleration pulse by Arbogast et al. (2009). The variation tendencies of shoulder/lap belt force curves of TUST IBMs 6YO agree well with those by Giordano et al. (2017), where simulations with the position and personalize advanced human body models for injury prediction (PIPER) scalable child model showed a greater maximum shoulder/lap belt force, and possible reasons could be associated with the muscle modeling method. The TUST IBMs 6YO thoracoabdominal muscle models with detailed anatomical structures were constructed based on the CT data of a 6YO child, which could better simulate the geometric characteristics and the direction of force transmission of the muscles, rather than using an equivalent muscle like that in the PIPER scalable child model.

The variation tendencies of the thorax acceleration, thorax deflection, shoulder belt force, and lap belt force curves of TUST IBMs 6YO are in good agreement with the corresponding curves of Q6 and V6. In addition, the difference between TUST IBMs 6YO, Q6, and V6 in acceleration and deflection in the thorax is caused by the different thorax structure of the models. The different response to the safety belt in the unloading stage of the thoracoabdominal contact force is caused by the impact of the simple seat model used in V6 during the unloading stage.

It can be seen from Figure 7 that the thorax deflections of TUST IBMs 6YO and V6 are greater than those of Q6, which is caused by the high thorax stiffness of Q6. Figures 8, 9 show that the maximum shoulder belt force of TUST IBMs 6YO is smaller than those of V6 and Q6, while the opposite is true for the lap belt force. The reason for the different simulation results of the three models is due to the different structure and geometry of the models. From Figures 7, 8, the value of thorax deflection of TUST IBMs 6YO was close to that of V6, while the value of shoulder belt force of TUST IBMs 6YO was smaller than that of V6 in the time interval 0–100 ms, which indicated that the thorax total stiffness of TUST IBMs 6YO was smaller than that of V6. It can also be seen that the thorax total stiffness of V6 was greater than that of Q6.

The thorax injury indexes include the viscosity criterion (V*C) and abbreviated injury scale (AIS). The V*C value represents the change rate of chest deformation relative to time (see Eq. 1), which is used to evaluate the damage to chest soft tissue.

$$V^{*}C = V(t)C(t) = \frac{d[D(t)]}{dt}\frac{D(t)}{b} \tag{1}$$

Here, $D(t)$ is the time function of chest compression and b is the initial chest thickness.

The correlation between (V*C)max and chest injury has been investigated in thoracic impact experiments with human cadavers in the literature (Viano, 1989; Cavanaugh et al., 1993; Pintar et al., 1997), which provides data support for the prediction of chest injury. Therefore, (V*C)max is used as an index to evaluate chest injury in this article. The chest injury

TABLE 4 Detailed information of injury threshold of the 6YO child.

Parameter	Chest $(VC)_{max}$	Abdomen $(VC)_{max}$	Abdomen $F_{max}C_{max}$
Scale factor	$0.6562^{1/2}$	$0.6562^{1/2}$	$0.642^{2} \times 0.6562$
Adult injury threshold	1.3 (m/s)	1.4 (m/s)	1540 (N)
Injury threshold of the 6YO child	1.053 (m/s)	1.134 (m/s)	417 (N)

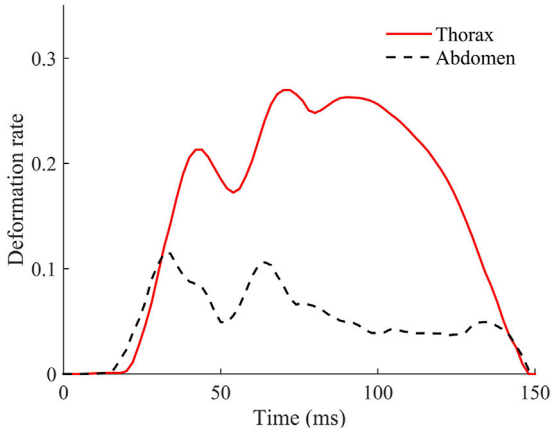

FIGURE 10
Thorax and abdomen deformation rate curves of TUST IBMs 6YO.

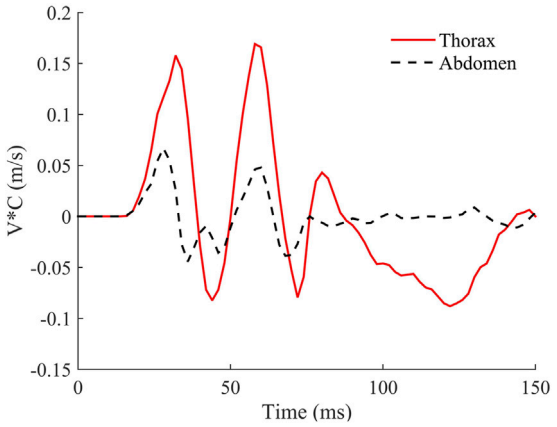

FIGURE 11
Thorax and abdomen V*C curves of TUST IBMs 6YO.

threshold (VC)max of lateral impacts was obtained from Ivarsson et al.'s (2004) study, and the relationship between injury threshold (VC)max of frontal impacts and lateral impacts was obtained from Viano et al.'s (1989) study. The chest and abdomen injury thresholds of frontal impacts are shown in Table 4.

The injury level formula is the relationship between the AIS and compression ratio of the chest and abdomen obtained by Viano et al. (1989), as shown in Eq. 2, where C is the chest compression index, which refers to the ratio between chest compression and chest thickness.

$$AIS = -3.78 + 19.56C \quad (2)$$

The ratio between the AIS of a 6YO child and the compression of the chest and abdomen is obtained according to the height ratio between children and adults as follows in Eq. 3.

$$AIS = -2.48 + 12.71C \quad (3)$$

The deformation rate, V*C, FmaxCmax of the thorax and abdomen, the trunk angle, and the maximum first principal strain of internal organs are obtained from the frontal sled simulation, as shown in Figure 10, Figure 11, Figure 12, Figure 13, and Figure 14. In addition, Table 5 shows the injury parameters of the thorax and abdomen for TUST IBMs 6YO.

From Figure 10 and Table 5, it can be seen that the maximum deformation rates of the chest and abdomen of TUST IBMs 6YO are 26.97 and 11.49%, respectively. According to Eq. 3, the thorax AIS of TUST IBMs 6YO is 0.925 with the maximum deformation rate of the chest 26.97%, which indicates that the child injury is mild in the frontal sled simulation. The maximum V*C values of the thorax and abdomen of TUST IBMs 6YO are 0.169 and 0.06, respectively, which do not reach the corresponding injury thresholds of 1.053 and 1.134, while the probability of AIS 4+ is 25% (Ivarsson et al., 2004), which indicates that the thorax and abdomen of TUST IBMs 6YO have a higher probability of slight or no injury. From Figures 10, 11, the maximum deformation rate and V*C values of the thorax are greater than those of the abdomen due to the difference in the effect of the seat belt on the thorax and abdomen.

The injury thresholds of the first principal strain of heart contusion and laceration were defined in this paper as 30% and 62.6 ± 6.9%, respectively, according to Yamada's (1970) study. The maximum first principal strain of the lungs (28.4%) was used to reflect pulmonary contusion, which was obtained by combining experiment and FE simulation results by Gayzik (2008). From Figures 12, 13, it is known that the maximum first principal strain of the heart is 11.8% at 68 ms, which is caused by the compression of the heart, sternum, and the fourth and fifth ribs under the seat belt. By comparing the maximum first principal strain and injury threshold of the heart, the result shows that there are no

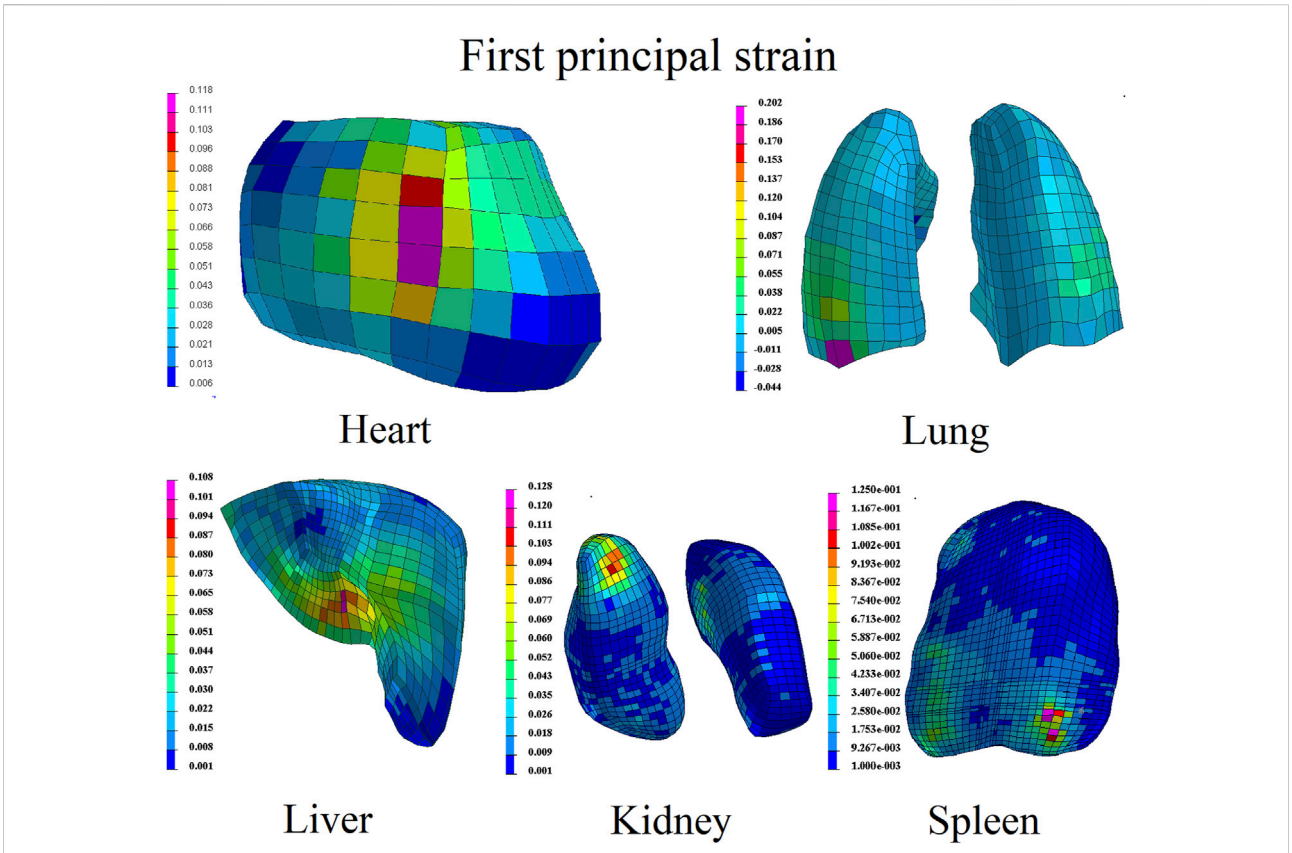

FIGURE 12
Maximum first principal strain diagrams of internal organs in TUST IBMs 6YO.

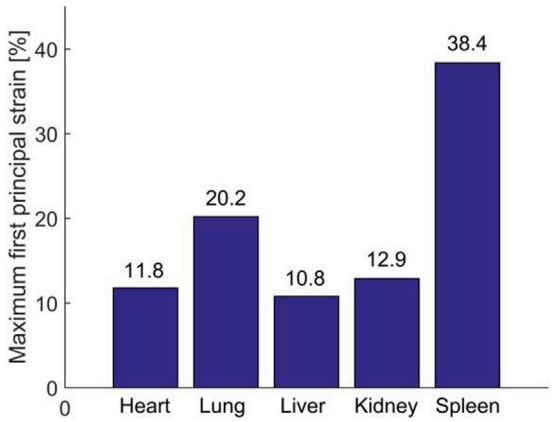

FIGURE 13
Maximum first principal strains of internal organs for TUST IBMs 6YO.

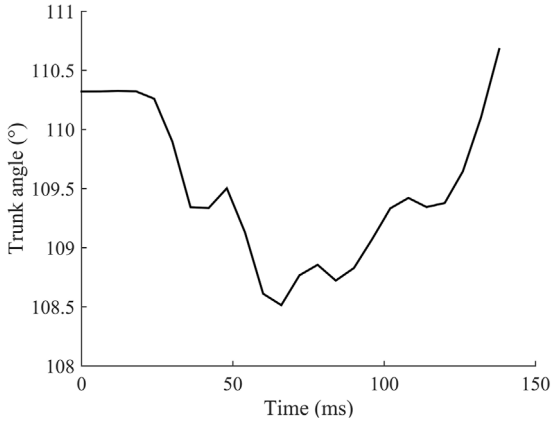

FIGURE 14
Trunk angle curve of TUST IBMs 6YO.

contusions or lacerations in the heart. The maximum first principal strain of the lungs is 20.2% at 38 ms, which does not reach the injury threshold (28.4%), and indicates that no pulmonary contusion occurred. The pressure of the safety belt is large during the motion process, which can easily cause lung damage from the ribs. Therefore, the safety belt cushion should be added in the

TABLE 5 Injury parameters of the thorax and abdomen for TUST IBMs 6YO.

Parameter	TUST IBMs 6YO	Injury Threshold
Chest (V^aC)max (m/s)	0.169	1.053[a]
Abdominal (V^aC)max (m/s)	0.06	1.134[a]
Chest AIS	0.925	-
Abdominal AIS	0	-
Chest compression rate (%)	26.97	-
Abdominal compression rate (%)	11.49	-
Chest FmaxCmax (N)	514.05	-
Abdominal FmaxCmax (N)	242.63	417**

[a]significant level: 0.01 ** significant level: 0.04.

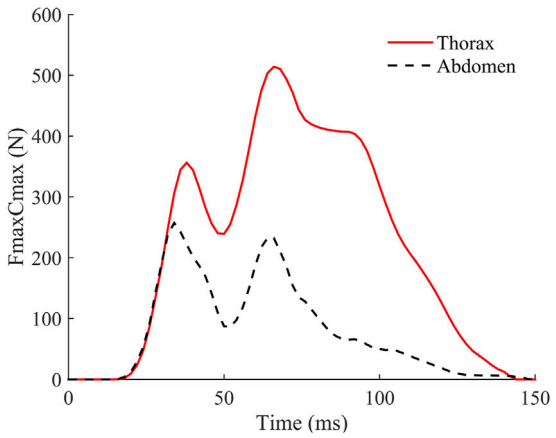

FIGURE 15
Thorax and abdomen FmaxCmax for TUST IBMs 6YO.

safety belt design, which can effectively reduce the damage to the lungs. The distributions of the first principal strain in the heart and lungs are consistent with those in the study by Tang (2018), where simulations with the THUMS 3YO occupant model showed a larger first principal strain, and possible reasons could be associated with the element type and boundary definition type. The heart and lungs in TUST IBMs 6YO were constructed using a hexahedral solid element rather than a tetrahedral solid element like that in the THUMS model. The boundary condition of the heart and lungs in TUST IBMs 6YO was defined as surface to surface contact, which could better simulate the actual boundary conditions, rather than using shared boundary node setting like that in the THUMS model. The tolerance value of the first principal strain of the liver was defined in this paper as 30% according to Melvin et al.'s (1973) study. The maximum first principal strain values of the liver, spleen, and kidney are 10.8% (at 38 ms), 38.39% (at 76 ms), and 12.9% (at 54 ms), respectively. The maximum first principal strain of the liver is smaller than the corresponding injury threshold, which indicates no injury to the liver. The maximum first principal strain values of the liver and kidneys are due to the extrusion of the liver/kidney and the stomach, while the maximum first principal strain of the spleen appears on account of the contact of the ribs with the spleen and the diaphragm under the action of the safety belt, see Supplementary Appendix SC. It can be seen from the data that the injury risks to internal organs of children such as the heart, lungs, liver, and kidneys during the kinematic response are lower, indicating that these organs are better protected than the spleen.

The definition of the trunk angle is the angle between the line of the hip joint and shoulder joint and the horizontal. From Figure 14, the maximum trunk angles are 108.51° and 110.67°. The greater the change in trunk angle, the more obvious the submarining trend, which represents a higher injury risk of the child's abdomen due to the compression of internal organs after the lap belt slipped over the iliac crests, which is consistent with the study by Adomeit and Heger, 1975. The abdomen is easily injured at 66 and 138 ms.

The FmaxCmax injury parameter value is a comprehensive injury evaluation index, which is obtained from the product of the maximum contact force between the thorax and the seat belt and the thorax compression ratio. The thorax injury risk increases with the increase of the FmaxCmax value. The experimental analysis by Untaroiu et al. (2012) shows that FmaxCmax and the intrusion speed of children's safety belts are the best indices to predict injury. Figure 15 shows the variation tendency of FmaxCmax of TUST IBMs 6YO. The maximum FmaxCmax value of the abdomen 240.63 N is smaller than the corresponding injury threshold 417 N obtained from Table 5, which indicates that there is no probability of AIS 4 + abdominal injury. The FmaxCmax value of the chest is greater than that of the abdomen in the time interval of 35–140 ms.

There are a few limitations to the study: 1) the study focuses on the specific topic of a 6YO thorax and abdomen comparison in a frontal sled test simulation. Future work could address thorax and abdomen injuries in lateral impact simulation. 2) Most of the material parameters of TUST IBMs 6YO are obtained by scaling those of the adult, which will be continuously updated as technology develops. 3) Injury thresholds for children were obtained by scaling the adult injury thresholds, which need to be further verified in future studies.

4 Conclusion

The paper demonstrates that the variation tendency of thorax acceleration, the intrusion of the thorax safety belt, and the shoulder/lap belt force in Q6, V6, and TUST IBMs 6YO are consistent with each other. The thorax total stiffness of the Q6, V6, and TUST IBMs 6YO models shows a decreasing trend. According to the injury index of the TUST IBMs 6YO in the motion process, it can be seen that the injury risks of the thorax and abdomen are relatively high at 80 ms, and better emergency measures should be provided to better protect the thorax and abdomen and reduce the injury. In addition, the child safety seat should be improved, addressing the injuries of the thorax and abdomen to achieve the best protection. The paper shows the greater advantages of the simulation output data of the child FE model with detailed anatomical structures to better reflect the performance of the child safety seat and provide more specific data for improving the CRS.

Data availability statement

The original contributions presented in the study are included in the article/Supplementary Material; further inquiries can be directed to the corresponding authors.

Author contributions

The author's contributions are as follows: HL was in charge of the whole trial; WL, LH, and BZ wrote the manuscript; HZ, SC, LH, and SR assisted with simulation calculation and analyses.

Funding

This work was supported by the National Natural Science Foundation of China (Grant No. 81471274, 81,371,360, and 81,201,015) and by the European Regional Development Fund-Project "Application of Modern Technologies in Medicine and Industry" (Fund No.CZ.02.1.01/0.0/0.0/17_048/0,007,280).

Conflict of interest

Author BZ was employed by Quadrant Space Science and Technology Company, Limited.

The remaining authors declare that the research was conducted in the absence of any commercial or financial relationships that could be construed as a potential conflict of interest.

Publisher's note

All claims expressed in this article are solely those of the authors and do not necessarily represent those of their affiliated organizations or those of the publisher, the editors, and the reviewers. Any product that may be evaluated in this article or claim that may be made by its manufacturer is not guaranteed or endorsed by the publisher.

Supplementary material

The Supplementary Material for this article can be found online at: https://www.frontiersin.org/articles/10.3389/ffutr.2022.890776/full#supplementary-material

References

Adomeit, D., and Heger, A. (1975). Motion sequence criteria and design proposals for restraint devices in order to avoid unfavorable biomechanic conditions and submarining. *Stapp Car Crash Conf.* 19, 139.

Arbogast, K. B., Balasubramanian, S., Seacrist, T., Maltese, M. R., Garcia-Espana, J. F., Hopely, T., et al. (2009). Comparison of kinematic responses of the head and spine for children and adults in low-speed frontal sled tests. *Stapp Car Crash J.* 53, 329–372. doi:10.4271/2009-22-0012

Beauchamp, L., Beuse, N., and Doyle, S. (2005). *Child restraint dynamic performance evaluation in a 48 km/h (30 mph) sled test*. Washington: NHTSA Technical report.

Beillas, P., Soni, A., Chevalier, M. C., et al. (2014). "Q6 dummy thoracic response and diagonal belt interactions: Observations based on dummy testing and human and dummy simulations," in Proceedings of the IRCOBI Conference Proceeding, Berlin, Germany, September 10–12, 2014. Paper IRC-14-39.

Cao, L. B., Chen, H., Ren, X. J., and Ou Yang, Z. G. (2010). Study on an integrated child safety seat. Applied Mechanics and Materials. *Trans. Tech. Publ.* 34, 517–522. doi:10.4028/www.scientific.net/amm.34-35.517

Cavanaugh, J. M., Zhu, Y., Huang, Y., et al. (1993). "Injury and response of the thorax in side impact cadaveric tests," in Proceedings of the 37th Stapp Car Crash Conference, San Antonio, TX, November 1, 1993, 199–221. SAE Paper #933127.

Cui, S. H., Chen, Y., Li, H. Y., Cao, D. C., and Ruan, S. J. (2015). Development and validation for the finite element model of child head. *J. Med. Biomechanics* 30 (5), 452. doi:10.3871/j.1004-7220.2015.05.452

Cui, S. H., Shan, L. L., Li, H. Y., He, L. U., Lyu, W. L., Ruan, S. J., et al. (2016). Development and validation of a 6-year-old occupant thorax finite element model and impact injury analysis. *Chin. J. Automot. Eng.* 6 (6), 418Chinese. doi:10.3969/j.issn.2095-1469.2016.06.05

Eggers, A., Schnottale, B., and Ott, J. (2015). "Sensitivity of Q10 and Q6 chest measurements to restraint and test parameters," in Proceedings of the 24th International Technical Conference on the Enhanced Safety of Vehicles, Gothenburg, Sweden, June 8–June 11, 2015.

Franz, U., and Graf, O. (2000). "Accurate and detailed LS-DYNA FE models of the US-and EUROSID: A review of the German fat project," in Proceedings of the 6th International LS-DYNA Conference, Dearborn, MI, April 9–April 11, 2000.

Gayzik, F. S. (2008). *Development of a finite element based injury metric for pulmonary contusion*. Winston-Salem: Wake Forest University.

Giordano, C., Li, X., and Kleiven, S. (2017). Performances of the PIPER scalable child human body model in accident reconstruction. *PLoS ONE* 12(11), e0187916. doi:10.1371/journal.pone.0187916

Han, Y., Pan, D., Ouyang, J., Qian, L., Mizuno, K., and Anguo Cang, A. (2017). Study of chest injuries to 3YO child occupants seated in impact shield and 5-point

harness CRSs. *Traffic Inj. Prev.* 19(3), 274–279. doi:10.1080/15389588.2017.1385780

Haut, R. C., and Atkinson, P. J. (1995). "Insult to the human cadaver patellofemoral jointEffects of age on fracture tolerance and occult injury," in Proceeding of the 39th Stapp Car Crash Conference, San Diego, CA, November 1, 1995, 39, 281.

Huang, Y., Ji, P. J., Ma, L. C., et al. (2016). A study on crash waveform dispersion and its effects on the responses of child restraint system. *Automot. Eng.* 38 (4), 440. doi:10.19562/j.chinasae.qcgc.2016.04.008

Hyncik, L., Cechova, H., Kovar, L., and Blaha, P. (2013). *On scaling virtual human models*. U.S. and Canada: SAE Technical Paper. 2013-01-0074.

Hyncik, L., Mana, J., Spicka, J., Špirk, S., and Kovar, L. B. (2014). *Development of 6 years old child virtual model by automatic scaling*. U.S. and Canada: SAE Technical Paper. 2014-01-2028.

Ivarsson, B. J., Crandall, J. R., and Longhitano, D. (2004). *Lateral injury criteria for the 6-year-old pedestrian - Part I: Criteria for the head, neck, thorax, abdomen and pelvis*. U.S. and Canada: SAE Technical Papers.

Jager, K. D., Ratingen, M. V., Lesire, P., Guillemot, H., Schnottale, B., Tejera, G., et al. (2005). "Assessing new child dummies and criteria for child occupant protection in frontal impact," in Proceedings of the 19th ESV conference, Washington, DC, June 6–June 9, 2005, TNO–LAB–BASt–IDIADA–UTAC.

Jiang, B. H., Cao, L. B., Mao, H. J., Wagner, C., Marek, S., and Yang, K. H. (2012). Development of a 10-year-old paediatric thorax finite element model validated against cardiopulmonary resuscitation data. *Comput. Methods Biomechanics Biomed. Eng.* 17 (11), 1185–1197. doi:10.1080/10255842.2012.739164

Jiang, B. H. (2013). *Development of finite element model and study of injury mechanisms for pediatric thorax*. Changsha: Hunan University.

Kajzer, J., Matsui, Y., Ishikawa, H., Günter, S., and Ulrich, B. (1999). *Shearing and bending effects at the knee joint at low-speed lateral loading*. Warrendale: SAE Special Publications.

Kerrigan, J. R., Ivarsson, B. J., Bose, D., Madeley, N. J., Millington, S. A., Bhalla, K. S., et al. (2003). ". Rate-sensitive constitutive and failure properties of human collateral knee ligaments," in Proceedings of the International Research Council on the Biomechanics of Impacts (IRCOBI) Conference, Lisbon (Portugal), September 25–26, 2022.

Kim, S., Ryu, H., Kim, Y., Baek, S., Kim, M., and Park, J. (2014). The study on the effect of seatbelt anchorage points using Q6 in sled test. *J. Auto-vehicle Saf. Assoc.* 6 (2), 49.

Li, H. Y., Cui, Z. Y., Cui, S. H., et al. (2017a). Development and validation of pelvic finite element model for a 6-year-old child. *Chin. J. Automot. Eng.* 7 (2), 100.

Li, H. Y., Li, K., Huang, Y. Q., Lv, W., Cui, S., He, L., et al. (2020). Validation of a finite element model with six-year-old child anatomical characteristics as specified in Euro NCAP Pedestrian Human Model Certification (TB024). *Comput. Methods Biomechanics Biomed. Eng.* 24 (6), 76–90. doi:10.1080/10255842.2020.1810677

Li, H. Y., Pan, Y. F., Ruan, S. J., et al. (2017b). Analysis of growth plate material property effect on knee injury of six-year-old child occupant. *Yiyong Shengwu Lixue/journal Med. Biomechanics* 32 (3), 213. doi:10.16156/j.1004-7220.2017.03.002

Luck, J. F., Nightingale, R. W., Yin, S., Kait, J. R., Loyd, A. M., Myers, B. S., et al. (2013). Tensile failure properties of the perinatal, neonatal, and pediatric cadaveric cervical spine. *Spine* 38 (1), E1–E12. doi:10.1097/brs.0b013e3182793873

Lv, W. L., Ruan, S. J., Li, H. Y., Cui, S., He, L.-J., and Wang, C.-X. (2016a). Development and validation of finite element model for 6-year-old pediatric neck. *J. Med. Biomechanics* 31 (2), 95–101. in Chinese. doi:10.3871/j.1004-7220.2016.02.095

Lv, W. L., Ruan, S. J., Li, H. Y., Cui, S., and He, L. (2015). Development and validation of a 6-year-old pedestrian thorax and abdomen finite element model and impact injury analysis. *Int. J. Veh. Saf.* 8 (4), 339–356. doi:10.1504/ijvs.2015.074378

Lv, W. L., Ruan, S. J., Li, H. Y., Cui, S. H., He, L. J., Wang, C. X., et al. (2016b). "Injury analysis of a six-year-old child pedestrian thorax in lateral/oblique impact," in Proceedings of the Eighth International Conference on Measuring Technology and Mechatronics Automation (ICMTMA), Macau, China, March 11–12, 2016: IEEE Computer Society, 352–358.

Lv, W. L., Ruan, S., Li, H. Y., Cui, S., and He, L. (2016c). Abdominal injury analysis of a 6-year-old pedestrian finite element model in lateral impact. *Int. J. Veh. Saf.* 9 (1), 85–100. doi:10.1504/ijvs.2016.077155

Maheshwari, J., Duong, N., Sarfare, S., and Belwadi, A. (2019). "Responses of a 6-year-old ATD restrained in a booster child seat on the FMVSS 213 test bench, proposed upgraded test bench and a vehicle seat in simulated frontal impacts," in Proceedings of the 26th International Technical Conference on The Enhanced Safety of Vehicles (ESV) - Conference Proceedings, Eindhoven, Netherlands, June 10–13, 2019.

Mañas, J., Kovář, L., Petřík, J., Čechová, H., and Špirk, S. (2012). Validation of human body model VIRTHUMAN and its implementation in crash scenarios. *Adv. Mech. Des.* 8, 351–356. doi:10.1007/978-94-007-5125-5_46

Melvin, J. W., Stalnaker, R. L., Roberts, V. L., et al. (1973). "Impact injury mechanisms in abdominal organs," in Proceedings of the 17th Stapp Car Crash Conference, Coronado, CA: Society of Automotive Engineers.

Mizuno, K., Iwata, K., Deguchi, T., Ikami, T., and Kubota, M. (2005). Development of a three-year-old child FE model. *Traffic Inj. Prev.* 6 (4), 361–371. doi:10.1080/15389580500255922

Nahum, A. M., Smith, R., and Ward, C. (1977). "Intracranial pressure dynamics during head impact," in Proceedings of 21st Stapp Car Crash Conference, New Orleans, LA: Society of Automotive Engineers 337–336.

Ouyang, J., Liu, C., Zhu, Q., Zhong, S., and Li, Z. (2015). Abdominal impact study on paediatric cadaveric subjects. *Int. J. Veh. Saf.* 8 (4), 287–298. doi:10.1504/ijvs.2015.074369

Ouyang, J., Xu, Y., Chen, W., Zhong, S., Zhu, Q., Zhao, W., et al. (2005). Biomechanical assessment of the pediatric cervical spine under bending and tensile loading. *Spine* 30 (24), E716–E723. doi:10.1097/01.brs.0000192280.53831.70

Ouyang, J., Zhao, W., Xu, Y., Chen, W., and Zhong, S. (2006). Thoracic impact testing of pediatric cadaveric subjects. *J. Trauma Inj. Infect. Crit. Care* 61 (6), 1492–1500. doi:10.1097/01.ta.0000233711.07823.40

Ouyang, J., Zhu, Q. A., Zhao, W. D., Xu, Y. q., Chen, W. s., and Zhong, S. z. (2003). Experimental cadaveric study of lateral impact of the pelvis in children. *1 Jun yi xue xue bao* 23 (5), 397.

Peng, L. Y. (2017). *Research on protective performance of child restraint system based on dummy, simulation and animal experiment*. China: Xiamen University of Technology. Master Thesis.

Pintar, F. A., Yoganandan, N., Hines, M. H., Maltese, M. R., McFadden, J., Saul, R., et al. (1997). "Chestband analysis of human tolerance to side impact," in Proceedings of the 41st Stapp Car Crash Conference, Lake Buena Vista, FL, November 12, 1997, 63–74. SAE Paper #973320.

Prange, M. T., Luck, J. F., Dibb, A., Van Ee, C. A., Nightingale, R. W., and Myers, B. S. (2004). Mechanical properties and anthropometry of the human infant head. *Stapp Car Crash J.* 48, 279–299. doi:10.4271/2004-22-0013

Q6 child dummy Model (2013). *Q6 child dummy Model*. Michigan: Humanetics. Release Version 1.0.

Shaw, J. M., Herriott, R. G., Mcfadden, J. D., Donnelly, B. R., and Bolte, J. H. (2006). Oblique and lateral impact response of the PMHS thorax. *Stapp Car Crash J.* 50 (1), 147.

Spicka, J., Manas, J., and Hyncik, L. (2015). Frontal impact response of a virtual low percentile six years old human thorax developed by automatic down-scaling. *Appl. Comput. Mech.* 9, 41. doi:10.4314/ahs.v3i3.6851

Tang, H. C. (2018). *Study on 3-year-old child occupant thoracic dynamic response and injury parameters in frontal impact*. China: Xiamen University of Technology. Master Thesis.

Trosseille, X., Cassan, F., and Schrooten, M. (2001). *Child restraint system for children in cars–CREST results*. U.S. and Canada: SAE Technical Paper.

Untaroiu, C., Darvish, K., Deng, B., and Wang, J. T. (2005). A finite element model of the lower limb for simulating pedestrian impacts. *Stapp Car Crash J.* 49 (11), 157. doi:10.4271/2005-22-0008

Untaroiu, C. D., Bose, D., Lu, Y. C., Riley, P., Lessley, D., and Sochor, M. (2012). Effect of seat belt pretensioners on human abdomen and thorax: Biomechanical response and risk of injuries. *J. Trauma Acute Care Surg.* 72 (5), 1304–1315. doi:10.1097/ta.0b013e3182472390

Viano, D. C. (1989).Biomechanical responses and injuries in blunt lateral impact," in Proceedings of the 33rd Stapp Car Crash Conference. U.S. and Canada: SAE Technical Paper, 113–142. SAE Paper #892432.

Viano, D. C., Lau, I. V., Asbury, C., King, A. I., and Begeman, P. (1989). Biomechanics of the human chest, abdomen, and pelvis in lateral impact. *Accid. Analysis Prev.* 21 (6), 553–574. doi:10.1016/0001-4575(89)90070-5

Vychytil, J., Manas, J., Cechova, J., et al. (2014). *Scalable multi-purpose virtual human model for future safety assessment*. U.S. and Canada: SAE Technical Paper. 2014-01-0534.

Yamada, H. (1970). *Strength of biological materials*. Baltimore: Williams & Wilkins.

Zhang, X. R., Wang, H. T., and He, J. (2021). Research on seat belt restraint path for child booster seats. *Chin. J. Automot. Eng.* 11 (1), 59–65. in Chinese.

Zhao, J. Z., and Norwani, G. (2007). Biomechanical analysis of hard tissue responses and injuries with finite element full human body model. *ESV Conf.* 9, 07.